Angewandte Chemie

A Journal of the Gesellschaft Deutscher Chemiker

International Edition

www.angewandte.org

Accepted Article

WILEY-VCH

RESEARCH ARTICLE

Engineering Nanoparticulate Organic Photocatalysts via a Scalable Flash Nanoprecipitation Process for Efficient Hydrogen Production

Miaojie Yu,[‡] Weiwei Zhang,[‡] Zhiqian Guo, Yongzhen Wu,* and Weihong Zhu*

[*]   M. Yu, Dr. W. Zhang, Prof. Z. Guo, Prof. Y. Wu, Prof. W. Zhu
        Key Laboratory for Advanced Material, Joint International Research Laboratory of Precision Chemistry and Molecular Engineering, Feringa Nobel Prize
        Scientist Joint Research Center, Shanghai Key Laboratory of Functional Materials Chemistry, Institute of Fine Chemicals, Frontiers Science Center for
        Materiobiology and Dynamic Chemistry, School of Chemistry and Molecular Engineering
        East China University of Science & Technology
        Shanghai 200237, P. R. China
        E-mail: whzhu@ecust.edu.cn; wu.yongzhen@ecust.edu.cn

[‡]   These authors are contributed equally

        Supporting information for this article is given via a link at the end of the document.

Abstract: Directly converting sunlight into hydrogen fuels using particulate photocatalysts represents a sustainable route for clean energy supply. Organic semiconductors have emerged as attractive candidates but always suffer from optical and exciton recombination losses with large exciton "dead zone" inside the bulk material, severely limiting the catalytic performance. Herein, we demonstrate a facile strategy that combines a scalable flash nanoprecipitation (FNP) method with hydrophilic soluble polymers (**PC-PEG5** and **PS-PEG5**) to prepare highly efficient nanosized photocatalysts without using surfactants. Significantly, a 70-fold enhancement of hydrogen evolution rate (HER) is achieved for nanosized **PC-PEG5**, and the FNP-processed **PS-PEG5** shows a peak HER rate of up to 37.2 mmol h^{-1} g^{-1} under full-spectrum sunlight irradiation, which is among the highest results for polymer photocatalysts. Moreover, a scaling-up production of nanocatalyst is demonstrated with the continuously operational FNP, which provides an unprecedented strategy toward practical applications of particulate photocatalysts for sustainable energy production.

Introduction

Converting sunlight into hydrogen fuel using particulate photocatalysts represents a facile and low-cost route for clean and sustainable energy supply.[1] Traditional photocatalysts are inorganic semiconductors with good solar-to-hydrogen efficiency while tuning their properties is challenging.[2] Recently, organic semiconductors have emerged as promising candidates for solar driven water splitting because of their diverse chemical structures and highly tunable optoelectronic properties.[3] The widely studied organic photocatalysts include families of materials known as graphitic carbon nitrides (g-C$_3$N$_4$),[4] linear conjugated polymers (LCPs),[5] conjugated microporous polymers (CMPs),[6] and covalent organic frameworks (COFs).[7] In spite of numerous efforts, the photocatalytic performance of organic semiconductors is still far away from application. As most studies focus on chemical structure engineering to modulate the absorption and energy levels of semiconductors, another predominated factor, the particle size of photocatalyst, was often overlooked.[8]

In general, learning from inorganic semiconductors, organic photocatalysts were usually dispersed by bath ultrasonication in water-dominated working system. However, due to the use of large aromatic building blocks, they are far less polar than inorganic counterparts, which results in bulky particles in water with size ranging from microns to millimeters (Figure 1a).[8-9] It is known that the length scale that light can penetrate organic photocatalysts is only tens to hundreds of nanometers because of their high molar extinction coefficient. The bulky particle size can thus cause apparent optical losses. In addition, due to the limited photo-generated exciton diffusion length (about 10 nm), many excitons inside the bulk materials (μm scale) can hardly transport to the surface of catalyst, leading to the formation of large exciton "dead zone".[10] Recently, several groups have independently revealed that decreasing the particle size of organic photocatalysts into a few to tens of nanometers could remarkably enhance their photocatalytic performance.[11] In essence, nanosized photocatalysts are more dispersible compared to bulk materials, thus not only enhancing light-harvesting but also facilitating exciton interception and dissociation at particle surface.[8, 11] The methods for acquiring organic nano-photocatalysts include physical exfoliation of two-dimensional crystalline materials (such as g-C$_3$N$_4$ and CMPs),[12] template-synthesis (g-C$_3$N$_4$ nanorods),[13] emulsion polymerization (insoluble CMPs and LCPs)[14] and nanoprecipitation of polymer dots (Pdots, soluble LCPs).[15] The design of water-soluble polymer and polyelectrolyte is also effective in attaining nanosized particles.[16] However, these strategies either lack a fine-control over particle size/morphology or rely on additional insulate surfactants, and nearly all these methods confront the difficulty of large-scale production, which criticaly obstructs their practical implements.

Synthetic modularity of organic semiconductors endows them with possibility of solution process. Generally, insoluble photocatalysts have their microstructure "fixed in" during synthesis, while soluble materials offer chances for post-synthetic modification. We here present a facile strategy that combines a couple of rationally designed hydrophilic soluble polymers (**PC-PEG5** and **PS-PEG5**) (Figure 1b) with a scalable flash
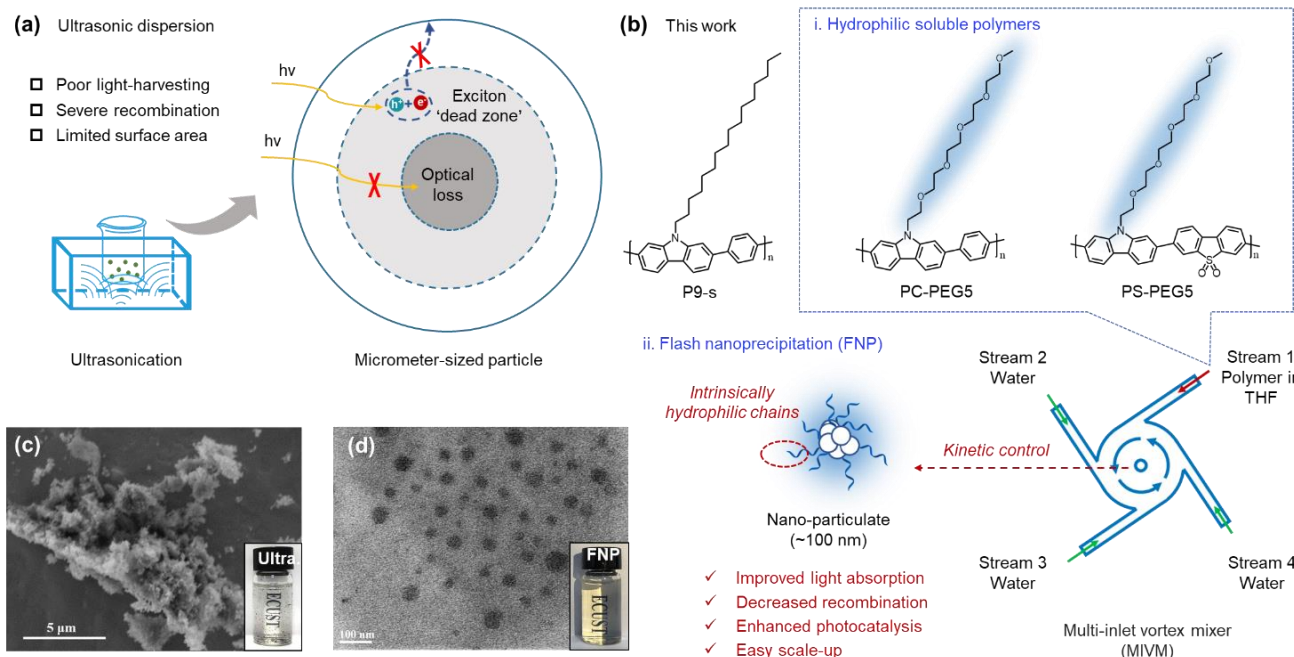
RESEARCH ARTICLE

Figure 1. (a) Schematic illustration of photocatalysts processed by bath ultrasonication; (b) Schematic illustration of photocatalysts processed by FNP; (c) Scanning electron microscope (SEM) image and digital photograph of bulky photocatalysts processed by bath ultrasonication (Ultra) showing micron-sized aggregates; (d) Transmission electron microscope (TEM) image and digital photograph of colloid solutions prepared by FNP method comprising uniformly distributed particles of tens of nanometers.

nanoprecipitation (FNP) technique to prepare nanoparticulate organic photocatalysts. By using FNP technology that implements a kinetical-control on particles formation, polymer photocatalysts can be solution-processed into homogenous and stable colloidal solutions comprising uniformly distributed particles with size of tens-to-hundred nanometers. Compared to the bulky particles suspension, a significant 70-fold improvement of hydrogen evolution rate (HER) was realized for FNP processed **PC-PEG5**, and **PS-PEG5** even achieves a peak HER of 37.2 mmol h^{-1} g^{-1} under full-spectrum light irradiation. The continuous operation and high reproducibility of FNP render this facile strategy with scale-up potential for practical application.

Results and Discussion

Grafting PEG side chains for hydrophilic soluble polymeric photocatalysts

P9-s is a polymer photocatalyst which was firstly developed by Cooper et. al.[17] The decorated long alkyl chains endow it with soluble characteristic but meanwhile hydrophobicity. Here we employed a molecular engineering to introduce a hydrophilic penta-(ethylene glycol) (PEG) side chain and dibenzothiophene sulfone ($DBTO_2$) unit into the conjugated backbone, and design two new polymers of **PC-PEG5** and **PS-PEG5**, respectively. The synthetic routes are shown in Scheme S1. All of these alternating co-polymers were synthesized using Pd(0)-catalyzed Suzuki-Miyaura polycondensation from hydrophobic alkyl or hydrophilic PEG side chains functionalized carbazole monomers with diboronic acid ester functionalized comonomers. The crude products were purified with methanol and acetone, and the soluble parts were collected using dichloromethane. We note that these polymers are soluble in common organic solvents like

tetrahydrofuran (THF) and chloroform, which facilitates further solution-based processes.

The chemical structures of the as-prepared polymers were characterized by elemental analysis, ^1H NMR and Fourier Transform Infrared (FT-IR) spectra. In FT-IR spectra, **P9-s** shows two characteristic C-H stretching vibration peaks attributed to alkyl chains at 2800-3000 cm^{-1}, whereas **PC-PEG5** and **PS-PEG5** exhibit weak signals for C-H vibration but new asymmetric stretching vibration peaks attributed to C-O-C in the range of 1000-1170 cm^{-1}, confirming the presence of PEG side chains (Figure S1). The molecular weights of **PC-PEG5** and **PS-PEG5** were estimated by gel permeation chromatography (GPC) and the results are summarized in Table S1. All polymers exhibited high thermal stability with a decomposition temperature ranging from 350 to 400 °C under N_2 atmosphere (Figure S2). The powder X-ray diffraction (PXRD) measurement suggests these polymers were amorphous in solid state (Figure S3).

The UV-vis absorption and emission spectra of the polymers were studied in dichloromethane (Figure S4-S6). **PC-PEG5** shows an absorption onset at 414 nm, with a slight red-shift relative to that of **P9-s** (403 nm). When the $DBTO_2$ group is introduced, a significant red-shift (57 nm) is observed for **PS-PEG5** due to the enhanced electron-withdrawing property of $DBTO_2$ group. The soluble characteristic of three polymers allowed us to investigate their energy levels using cyclic voltammetry analysis (Figure S7-S8). The highest occupied molecular orbit (HOMO) levels of **P9-s**, **PC-PEG5** and **PS-PEG5** are similar (-5.73, -5.70 and -5.72 eV versus vacuum, respectively), while the lowest unoccupied molecular orbital (LUMO) levels of **PS-PEG5** (-3.09 eV versus vacuum) is more negative than that of **P9-s** and **PC-PEG5** (-2.66 and -2.71 eV versus vacuum), which can be attributed to the introduction of strong electron-withdrawing $DBTO_2$ unit. The measured LUMO
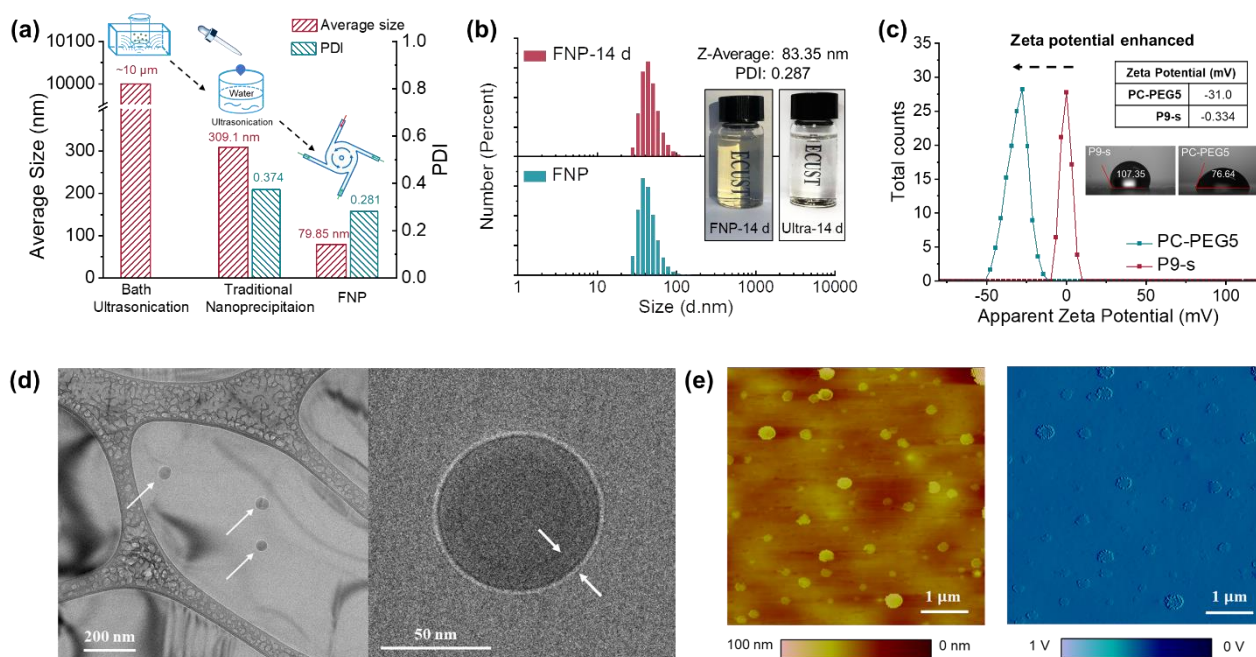
RESEARCH ARTICLE

Figure 2. (a) Comparation of average size and poly dispersion index (PDI) of particles for samples processed by bath ultrasonication, traditional nanoprecipitation and FNP; (b) Dynamic Light Scattering (DLS) results for initial **PC-PEG5** nanoparticles and after 14 days (inserts are digital photographs of samples processed by ultrasonication (Ultra) and FNP kept for 14 days); (c) Zeta potentials of **P9-s** and **PC-PEG5** samples processed by bath ultrasonication and FNP method at pH 7.4 (inserts are water contact angles of **P9-s** and **PC-PEG5**); (d) Cryo-transmission electron microscopy (Cryo-TEM) images of **PC-PEG5** nanoparticles prepared by FNP; (e) Atomic force microscopy (AFM) image of **PC-PEG5** nanoparticles prepared by FNP (left image is a height map and right image is an adhesion map).

levels for all as-prepared polymers are thermodynamically high enough for proton reduction.

The hydrophilic properties of the three polymers were tested by water contact angle measurement on their spin-coating films (Figure 2c and S9). Compared with **P9-s** (107.35°), the water contact angles of **PC-PEG5** (76.64°) and **PS-PEG5** (74.63°) are largely decreased, indicating that the substitution of alkyl side chains by PEG side chains can dramatically improve the hydrophilicity of conjugated polymers. Namely, better interfacial wettability with water is realized for PEG functionalized polymer catalysts.

Kinetically controlled production of stable nanoparticulate colloid via FNP

So far, bath ultrasonication is the most widely used method to disperse photocatalysts, where the bulky powder materials are dispersed using fierce conditions for a proper working suspension. We firstly dispersed the **PC-PEG5** with bath ultrasonication, which generated mixture with naked-eye visible particles, and the particle sizes are in the range of micrometers (Figure 1c). These bulky particles are found to quickly sunk to the bottom (Figure 2b), and the suspension should be kept in stirring to prevent unfavorable sedimentation during the photocatalytic reaction.[18]

To minimize the particle size of the photocatalyst, some nanoprecipitation methods were previously reported for preparing nano-sized catalysts. They were usually conducted by hand injection of polymer solution into a large amount of water with vigorous stirring or bath ultrasonication.[15] In this process, the time scale of solvent mixing (τ_{mix}) is much longer than that of hydrophobic portion nucleation ($\tau_{N.G.}$) and hydrophilic portion aggregation (τ_{agg}), resulting in a thermodynamically dictated nanoparticles (NPs) formation.[19] As a consequence,

polydisperse NPs are often generated, and extra filtration is necessary to exclude the big aggregates, which causes decreased throughput and unfavorable wastes.[20]

In contrast, FNP technique employs a multi-inlet vortex mixer (MIVM) system where the organic solvent dramatically mixes with antisolvent (water) in the range of milliseconds.[21] The τ_{mix} in FNP process is shorter than the characteristic nucleation time of polymers, and the growth of the NPs is thus a kinetically controlled process, which could generate nanoparticles with uniform dispersion and small particle size. Moreover, the particle size can be modulated by changing the flow rates of different streams. Here we have for the first time employed FNP technique to prepare nanoparticulate photocatalysts. As seen from Figure 1d, it produced a clear colloidal solution with the uniformly dispersed spherical particles ranging from 40 to 100 nm. The average particle size and poly dispersion index (PDI) of resulting nanoparticles were 79.85 nm and 0.281, respectively, as indicated by Dynamic Light Scattering (DLS) (Figure 2a). As a contrast, traditional nanoprecipitation method was also performed by directly injecting the THF solution of **PC-PEG5** into water while ultrasonication. The resulting solution is measured to have broader size distribution (0.374) with a larger particle size (309.1 nm) relative to FNP (Figure 2a and S10). The stability of the FNP-produced colloidal solution was evaluated by keeping **PC-PEG5** solution unruffled for over 14 days. The solution was found to remain clear with average particle diameter and size polydispersity barely changed in DLS measurement (Figure 2b), indicating that the **PC-PEG5** nanoparticles can be stable in water.

When it comes to the alky chains based **P9-s**, FNP method can generate a homogeneous dispersion as well. However, the average particle size reaches 865.3 nm, distinctly larger than PEG functionalized **PC-PEG5** (Figure S11). After removing THF, the particles gradually aggregated and finally settled out to be

RESEARCH ARTICLE

macroscopic bulk particles (Figure S12). The dispersion stability was testified by Zeta potentials characterization. As shown in Figure 2c, the Zeta potential of **P9-s** particles was -0.334 mV, while that of the hydrophilic **PC-PEG5** was much more negative (-31.0 mV), implying that PEG chains can provide electrostatic stabilization for the nanoparticles. These remarkable differences manifest that the side chains play a critical role in the formation and stabilization of organic nanoparticles during FNP. We consider that the hydrophilic side chains in **PC-PEG5** tend to surround the polymer backbone and closely contact with water, which block the particle growth and thus result in small particle size with long-term stability.

The self-assembled morphology of nanoparticulate **PC-PEG5** was analyzed by cryo-transmission electron microscopy (cryo-TEM), which can image the samples in an environment that is very close to native state.[22] As shown in Figure 2d, an apparent double-layered sphere structure can be observed for the nanoparticles, suggesting the different densities between outside and inside, and this difference is probably related to exposed hydrophilic PEG side chains on the surface of particles. Further indicated by atomic force microscopy (AFM), the height map exhibits that the outer region of the sphere has different height with the central, and the adhesion mapping also shows corresponding variation from the outer to central region (Figure 2e). The outer layers composed of hydrophilic PEG chains could serve as a solvation layer to inhibit unfavorable aggregation of particles by steric repulsion, thus contributing to the high colloidal stability. Different from previous fabrication of polymer dots that additional surfactants were required to prevent aggregation, we directly prepared stable nanoparticulate organic catalysts via a combination of molecular engineering with FNP technique.

Enhanced photocatalytic performance of nanoparticulate catalysts

Photocatalytic hydrogen production experiments were carried out with ultrasonication and FNP-processed **PC-PEG5** as photocatalyst, ascorbic acid (AA) as sacrificial agents, and no additional platinum was loaded as cocatalyst. As exhibited in Figure 3a, 5 mg ultrasonic-dispersed **PC-PEG5** generated 8.8 μmol H_2 in 5 hours under full-spectral illumination, corresponding to a hydrogen evolution rate (HER) of 0.35 mmol h^{-1} g^{-1}. Under the same catalytic conditions, remarkably, the FNP processed **PC-PEG5** produced 204 μmol H_2, achieving an average HER of 8.2 mmol h^{-1} g^{-1}. An exceptional HER of 25.3 mmol h^{-1} g^{-1} was observed in the first hour, which is 72-fold higher than that of ultrasonic-dispersed samples. The apparent quantum yield (AQY) of **PC-PEG5** nano-photocatalyst was estimated to be 5.3% at 365 nm (Figure 3b and Table S3), which is around 30 times higher than bulky counterparts (0.18%). Several batches of **PC-PEG5** nanoparticles were reproduced by FNP using the same fabrication parameters, and there were negligible differences in the average particle size and photocatalytic activity among different batches (Figure S13-S14), demonstrating a high repeatability of this effective method. We also tried triethanolamine (TEOA) as the sacrificial agents and observed similar trend between FPN and ultrasonication-based samples (Figure S15).

Owing to the fine adjustability of the FNP technique, we further investigated the impact of particle sizes on the photocatalytic activity which was rarely studied. **PC-PEG5** nanoparticles with sizes ranging from 60 nm to 120 nm can be

facilely produced by altering the velocity of streams and concentration of polymer in THF. Detailed results are summarized in Table S4 and Figure S16-S17. As shown in Figure 3a, for 62, 80, 92, and 122 nm-sized photocatalyst, the eventually total amount of hydrogen generation is 228, 204, 199, 188 μmol in 5 hours operation, respectively. The photocatalytic activity is increased along with the decrease of particle size. Herein, we note that the HER variation for particle size changing in nanoscale is much smaller than that for particle size changing from micrometer to nanometer (from 0.35 to 25.3 mmol h^{-1} g^{-1}).
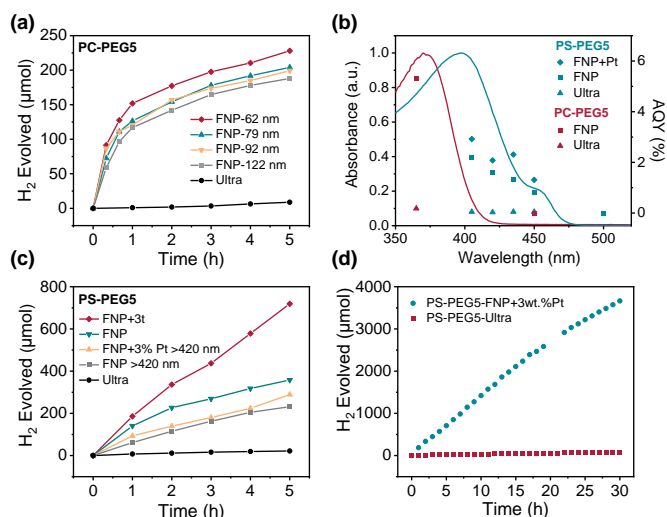

Figure 3. (a) Time-dependent photocatalytic hydrogen evolution for **PC-PEG5** nanoparticles with different sizes prepared by FNP and bath ultrasonication (Ultra) under full-spectral illumination; (b) The absorption spectra (lines) and AQYs (triangles, squares and diamonds) for **PC-PEG5** and **PS-PEG5** prepared by bath ultrasonication and FNP at 365, 405, 420, 450 and 500 nm, respectively; (c) Time-dependent photocatalytic hydrogen evolution for **PS-PEG5** prepared by FNP and bath ultrasonication under full-spectral illumination; (d) Long-term photocatalytic hydrogen evolution for **PS-PEG5** prepared by bath ultrasonication and FNP under full-spectral illumination.

To confirm the photocatalytic function with these designed polymers, control experiments were conducted by removing irradiation, polymer nanoparticles, or sacrificial agent, respectively. As shown in Figure S18, no detectable amount of hydrogen can be observed under these conditions. To exclude the influence of slight THF residue (in FNP-processed solutions) on photocatalysis, we also examined the mixture of THF/AA in water without **PC-PEG5**, and no H_2 was produced for this system under irradiation. All these results indicate that hydrogen production is photocatalysis rather than the decomposition of polymers, sacrificial agents, or the residual THF. After a 5 hours course of continuous photocatalysis experiment, we recycled the photocatalyst, and characterized it by UV-vis, ^1H NMR spectra and FTIR spectroscopy (Figure S19). No apparent change can be observed compared to pristine material, indicating that the photocatalyst is chemically stable under the working conditions.

Although **PC-PEG5** nanoparticles can achieve a considerable HER under full-spectrum light irradiation, no photocatalytic activity was observed for this polymer under visible light. Considering that the UV region comprises only 5% of solar energy,[51] it is highly desirable to expand the absorption range. As a demonstration, we have designed and synthesized another soluble polymer **PS-PEG5** that bears a strong electron-withdrawing unit $DBTO_2$, which exhibits a broadened absorption spectrum (Figure S6). Owing to the solution-processable and

4

RESEARCH ARTICLE

intrinsically hydrophilic property, **PS-PEG5** was also easily processed into nanoparticles via FNP method without using surfactants (Figure S20-S21). Remarkably, 5 mg **PS-PEG5** nano-photocatalyst produced 358 µmol hydrogen during 5 hours operation under full-spectrum light illumination (Figure 3c), achieving an average HER of 14.3 mmol h^{-1} g^{-1}. Furthermore, the HER in the first hour reaches 28.1 mmol h^{-1} g^{-1}, around 32 times higher than the ultrasonication based samples (0.87 mmol h^{-1} g^{-1}). We also processed the **PS-PEG5** with traditional nanoprecipitation method by directly injecting the THF solution of polymer into water with ultrasonic bath. As indicated in DLS result (Figure S20), the resulted solution shows an apparent peak at 1000 nm and much increased average particle size and PDI (1439 nm and 0.847), which is consistent with the variable-sized particles observed in its TEM image (Figure S21). Moreover, the traditional nanoprecipitation method prepared solution exhibits a broad and week absorption peak similar to the solid, while the absorption spectra of FNP sample approximate to the solution (Figure S22). Due to the polydisperse particles with larger diameters, traditional nanoprecipitation method processed **PS-PEG5** shows a poorer photocatalytic activity than FNP counterpart, with an average HER of 4.1 mmol h^{-1} g^{-1} in the five hours operation (Figure S23). In view of the high colloidal stability of FNP-processed **PS-PEG5**, we made an attempted to remove the stirring in photocatalytic operation. Interestingly, there is no deterioration of photocatalytic activity for the static solution with respect to the stirring one (Figure S24). It is thus the FNP derived nanoparticulate photocatalyst with uniform dispersion could increase the opportunities for a more energy-efficient photocatalytic hydrogen evolution system. With addition of 3 wt.% Pt as cocatalysts, the average HER can be further improved to 28.8 mmol h^{-1} g^{-1}, and a remarkable rate of 37.2 mmol h^{-1} g^{-1} for the initial hour (Figure 3c). This photocatalytic HER activity is among the highest reported for polymer photocatalysts (Table S5). Under visible light irradiation (> 420 nm), a notable HER of 11.6 mmol h^{-1} g^{-1} was achieved.

The AQYs of FNP prepared **PS-PEG5** at 405, 420, 435 and 450 nm were estimated to be 2.20, 1.60, 1.32, and 0.83%, respectively, about 44, 53, 26 and 17 times higher than that of ultrasonically dispersed sample, respectively (Figure 3b and Table S3). With additional 3 wt.% Pt as cocatalyst, these AQYs can be further increased to 2.92, 2.08, 2.31, and 1.31, respectively. Previously, it was reported that nano-photocatalysts often suffer from low stability, and many researches show deactivation of catalytic reaction after only a few hours.[15a-e] Here, the longer-term photocatalysis experiments for FNP processed nano-catalysts were operated up to 30 hours under full-spectrum light irradiation (Figure 3d). **PS-PEG5** shows high stability with an HER of last hour to be 18.1 mmol h^{-1} g^{-1}, which is 35-fold higher than that of the sample prepared by traditional bath ultrasonication (0.52 mmol h^{-1} g^{-1}). The enhanced stability for FNP-produced nano-photocatalyst can be correlated with the high colloidal stability of intrinsically hydrophilic polymer with well dispersion.

Insights into the improved photocatalytic activity for FNP-processed nano-catalysts

We then take insights into the improved photocatalytic performances for FNP-processed nanoparticles. Light-harvesting is one of predominated factors for photocatalytic reaction as the semiconductor firstly absorbs photons with sufficient energy to generate bound electron-hole pairs (excitons).[11] As depicted in Figure 4a, when dispersing polymers for same concentration, the ultrasonically dispersed sample displays a transmittance larger than 80% in the range of 300 to 450 nm, while less than 10% of the light can pass through the FNP-processed solution. Namely, minimizing the particle size from microscale to nanoscale can significantly enhance the light-harvesting, which can be the primary reason for the enhanced photocatalysis.

Scanning transmission electron microscopy (STEM) imaging with element analysis were employed to give insights into the structures of Pt-loaded nano-photocatalysts. As shown in Figure S25, a number of spherical nanosized particles with a diameter of around 100 nm can be observed for FNP processed **PS-PEG5**, while only bulky particle with size around 10 µm can be found for ultrasonically dispersed **P9-s** in the same magnification. The better dispersion with increased surface area is suposed to be favorable for cocatalysts loading. On the surface of **PS-PEG5** nanoparticles, the Pt cocatalysts were loaded with the sizes ranging from 5 to 10 nm (bright light parts) which were verified by element mapping (Figure 4b-4c). The distribution of Pt cocatalysts is prone to overlap with the signal of element O, which could be ascribed to the high affinity of oxygen-contained outside PEG chains with metal Pt.[24] Accordingly, **PS-PEG5** with PEG chains exposed at surface might bind more intimately with Pt compared to alkyl-functionalized polymer, facilitating the charge transfer from the polymers to the cocatalysts (discuss later).
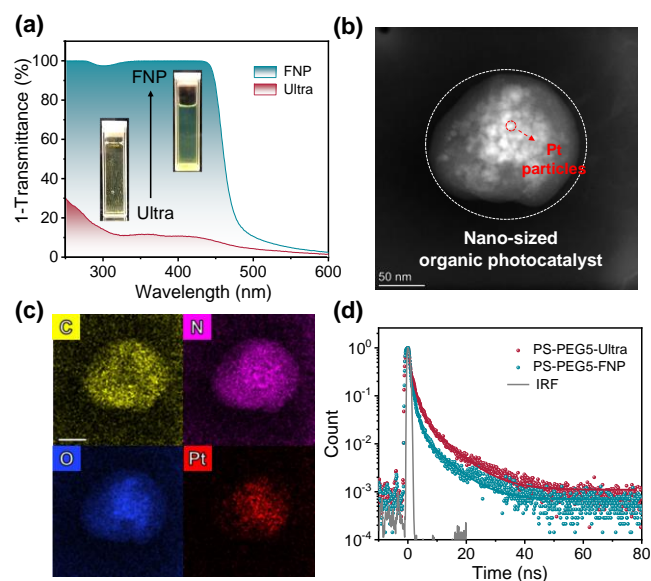

Figure 4. (a) Transmittance spectra of **PS-PEG5** processed by bath ultrasonication and FNP; (b) High-angle annular dark field-scanning transmission electron microscopy (HAADF-STEM) image for **PS-PEG5** nanoparticles prepared by FNP; (c) Element mapping for **PS-PEG5** nanoparticles prepared by FNP (all scale bars in C are 50 nm); (d) Time-resolved photoluminescence (TRPL) spectra for **PS-PEG5** in water processed by bath ultrasonication and FNP (excitation wavelength at 372 nm and detected wavelength at 470 nm).

The effect of particle size on the charge transfer process was studied by time-resolved photoluminescence (TRPL) decay with **PS-PEG5** prepared by FNP and bath ultrasonication, respectively. The decay traces are illustrated in Figure 4d, and the lifetimes were obtained by fitting the resulting curves with a tri-exponential model (Table S6). The average PL lifetimes (τ) were calculated to

5

RESEARCH ARTICLE

be 2.48 and 3.51 ns for FNP and ultrasonication prepared samples, respectively. The shortening of PL lifetime associated with the decrease of particle size can be attributed to the enhanced exciton quenching, which mainly occurs at particle surface by metal cocatalyst or surrounding water and sacrificial agent.[25] We here attribute the accelerated exciton quenching to both oxygen-contained PEG-chains that facilitate Pt cocatalyst loading and the smaller size of photocatalyst where the photo-generated excitons have much larger opportunities to reach the surface-dominated reaction sites. To sum up, the significantly improved photocatalytic performance for FNP-produced nanoparticulate catalyst is ascribed to the following factors: i) improved light harvesting; ii) facilitated cocatalyst loading as active sites; iii) enhanced exciton dissociation.

Scalable production of nanoparticulate photocatalysts with high reproducibility

Some useful strategies have previously reported for preparing nano-scaled organic photocatalysts with enhanced catalytic activity, such as surfactants involved polymer dots (Pdots) fabrication. However, the scalable production remains a great challenge for these strategies due to the discontinuous production, batch to batch sensitivity, and relatively low production yields. One key advantage of the FNP technique is the continuous operation, which can work as a promising route toward scalable production of nano-photocatalysts. The arrangement of FNP equipment is presented in Figure 5a. Water and polymer solution are pushed into a multi-inlet vortex mixer (MIVM) through four inlet streams and the resulting solution can be obtained immediately. As a demonstration, we multiplied the solution volume from initial 25 mL to 100, 500, 1000 mL using continuous FNP processing on **PS-PEG5** (Figure 5b). DLS results indicate the particles sizes in these solutions were almost identical (Figure 5c and Table S7), suggesting a stable production with high reproducibility. When randomly taking the same amount of solution (25 mL) from these different batches for photocatalytic hydrogen evolution test, they exhibited parallel photocatalytic activities (Figure 5d and Figure

S27-S28). These results indicate that FNP-produced organic nanoparticulate photocatalysts is scalable without deterioration of catalytic activity.

Conclusion

Given the significant optical loss with large exciton "dead zone" for bulk organic photocatalysts, we have for the first time introduced an effective strategy combining a scalable flash nanoprecipitation (FNP) method with hydrophilic soluble polymers to prepare nanoparticulate organic photocatalysts with boosted catalytic activity. The rational molecular design afforded two hydrophilic copolymers (**PC-PEG5** and **PS-PEG5**) that are soluble in organic solvents and easy for solution-processing. By using a kinetically controlled FNP method, the homogenous and stable colloidal solutions comprising uniformly distributed nanosized organic photocatalysts were successfully prepared without using surfactants. Significantly, a 70-fold enhancement of hydrogen evolution rate (HER) was realized for nanoparticulate **PC-PEG5**, and **PS-PEG5** even achieves a peak HER of 37.2 mmol h^{-1} g^{-1} under full-spectrum light irradiation, which is one of the highest results for polymer photocatalysts. The significantly improved photocatalytic performance for FNP-produced nano-catalyst is well ascribed to the improved light-harvesting, facilitated cocatalyst loading, and enhanced exciton dissociation. Based on the continuously operational FNP, a preliminary scaling-up production of photocatalytic solution has been demonstrated which avoids the traditional disadvantages such as the discontinuous production, batch to batch sensitivity, and relatively low production yields, thus offering an attractive protocol for massive production of nano-catalysts for practical implements. We expect that the strategy can provide a new platform to developing efficient nanoparticulate organic photocatalysts for photocatalytic hydrogen evolution, overall water splitting, and other solar-to-chemical energy conversions such as CO_2 reduction.[26]
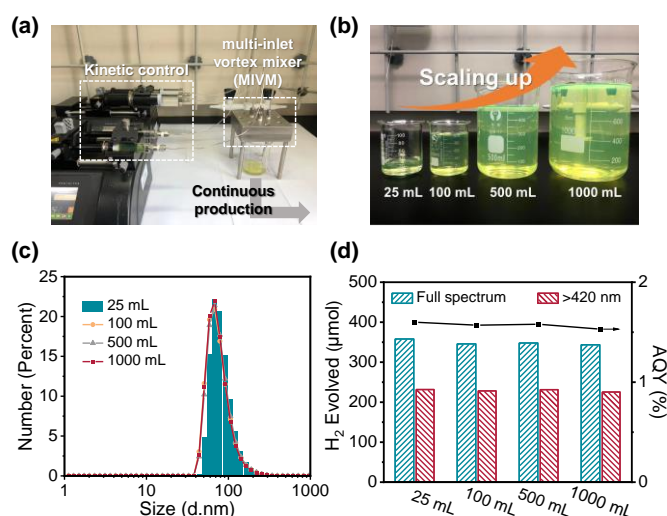
Figure 5. (a) Digital photograph of FNP instrument; (b) Digital photograph of 25, 100, 500 and 1000 mL solutions of **PS-PEG5** nanoparticle prepared by FNP; (c) DLS results and (d) amount of hydrogen evolved evolution and AQYs of 25 mL solution randomly taken from the initial 25 mL and 100, 500, 1000 mL solutions by continuous FNP operation on **PS-PEG5**.

[1] a) T. Hisatomi, K. Domen, *Nat. Catal.* **2019**, *2*, 387-399; b) Z. Wang, C. Li, K. Domen, *Chem. Soc. Rev.* **2019**, *48*, 2109-2125.

[2] Y. Wang, A. Vogel, M. Sachs, R. S. Sprick, L. Wilbraham, S. J. A. Moniz, R. Godin, M. A. Zwijnenburg, J. R. Durrant, A. I. Cooper, J. Tang, *Nat. Energy* **2019**, *4*, 746-760.

[3] C. Dai, B. Liu, *Energy Environ. Sci.* **2020**, *13*, 24-52.

[4] a) D. J. Martin, K. Qiu, S. A. Shevlin, A. D. Handoko, X. Chen, Z. Guo, J. Tang, *Angew. Chem. Int. Ed.* **2014**, *53*, 9240-9245; b) L. Lin, Z. Lin, J. Zhang, X. Cai, W. Lin, Z. Yu, X. Wang, *Nat. Catal.* **2020**, *3*, 649–655; c)

6

RESEARCH ARTICLE

X. Wang, K. Maeda, A. Thomas, K. Takanabe, G. Xin, J. M. Carlsson, K. Domen, M. Antonietti, *Nat. Mater.* **2009**, *8*, 76-80; d) W. Jiang, H. Wang, X. Zhang, Y. Zhu, Y. Xie, *Sci. China Chem.* **2018**, *61*, 1205-1213.

[5] a) R. S. Sprick, B. Bonillo, R. Clowes, P. Guiglion, N. J. Brownbill, B. J. Slater, F. Blanc, M. A. Zwijnenburg, D. J. Adams, A. I. Cooper, *Angew. Chem. Int. Ed.* **2016**, *128*, 1824-1828; b) X. Zhang, X. Wang, J. Xiao, S. Wang, D. Huang, X. Ding, Y. Xiang, H. Chen, *J. Catal.* **2017**, *350*, 64-71; c) Z. A. Lan, G. Zhang, X. Chen, Y. Zhang, K. A. I. Zhang, X. Wang, *Angew. Chem. Int. Ed.* **2019**, *58*, 10236-10240. d) Y. Bai, D. J. Woods, L. Wilbraham, C. M. Aitchison, M. A. Zwijnenburg, R. S. Sprick, A. I. Cooper, *J. Mater. Chem. A* **2020**, *8*, 8700-8705. e) C. Han, P. Dong, H. Tang, P. Zheng, C. Zhang, F. Wang, F. Huang, J. X. Jiang, *Chem. Sci.* **2021**, *12*, 1796-1802

[6] a) R. S. Sprick, J. X. Jiang, B. Bonillo, S. Ren, T. Ratvijitvech, P. Guiglion, M. A. Zwijnenburg, D. J. Adams, A. I. Cooper, *J. Am. Chem. Soc.* **2015**, *137*, 3265-3270; b) L. Li, Z. Cai, Q. Wu, W. Y. Lo, N. Zhang, L. X. Chen, L. Yu, *J. Am. Chem. Soc.* **2016**, *138*, 7681-7686; c) Z.-A. Lan, W. Ren, X. Chen, Y. Zhang, X. Wang, *Appl. Catal. B: Environ.* **2019**, *245*, 596-603; d) X. Gao, C. Shu, C. Zhang, W. Ma, S. Ren, F. Wang, Y. Chen, J. H. Zeng, J.-X. Jiang, *J. Mater. Chem. A* **2020**, *8*, 2404-2411; e) Y. Xu, C. Zhang, P. Mu, N. Mao, X. Wang, Q. He, F. Wang, J. Jiang, *Sci. China Chem.* **2017**, *60*, 1075-1083. f) A. M. Elewa, M. H. Elsayed, A. F. M. El-Mahdy, C. L. Chang, L. Y. Ting, W. C. Lin, C. Y. Lu, H. H. Chou, *Appl. Catal. B-Environ.* **2021**, *285*, 119802.

[7] a) P. Pachfule, A. Acharjya, J. Roeser, T. Langenhahn, M. Schwarze, R. Schomacker, A. Thomas, J. Schmidt, *J. Am. Chem. Soc.* **2018**, *140*, 1423-1427; b) W. Chen, L. Wang, D. Mo, F. He, Z. Wen, X. Wu, H. Xu, L. Chen, *Angew. Chem. Int. Ed.* **2020**, *59*, 16902-16909; c) J. Wang, J. Zhang, S. B. Peh, G. Liu, T. Kundu, J. Dong, Y. Ying, Y. Qian, D. Zhao, *Sci. China Chem.* **2019**, *63*, 192-197; d) Q. Liao, W. Xu, X. Huang, C. Ke, Q. Zhang, K. Xi, J. Xie, *Sci. China Chem.* **2020**, *63*, 707-714; e) X. Wang, L. Chen, S. Y. Chong, M. A. Little, Y. Wu, W. H. Zhu, R. Clowes, Y. Yan, M. A. Zwijnenburg, R. S. Sprick, A. I. Cooper, *Nat. Chem.* **2018**, *10*, 1180-1189.

[8] C. M. Aitchison, R. S. Sprick, *Nanoscale* **2021**, *13*, 634-646.

[9] a) D. J. Woods, S. A. J. Hillman, D. Pearce, L. Wilbraham, L. Q. Flagg, W. Duffy, I. McCulloch, J. R. Durrant, A. A. Y. Guilbert, M. A. Zwijnenburg, R. S. Sprick, J. Nelson, A. I. Cooper, *Energy Environ. Sci.* **2020**, *13*, 1843-1855; b) Y. Bai, Z. Hu, J. X. Jiang, F. Huang, *Chem. Asian J.* **2020**, *15*, 1780-1790.

[10] O. V. Mikhnenko, P. W. M. Blom, T. Nguyen, *Energy Environ. Sci.* **2015**, *8*, 1867-1888.

[11] C. H. Dai, Y. T. Pan, B. Liu, *Adv. Energy Mater.* **2020**, *10*, 2002474.

[12] a) L. Wang, Y. Wan, Y. Ding, S. Wu, Y. Zhang, X. Zhang, G. Zhang, Y. Xiong, X. Wu, J. Yang, H. Xu, *Adv. Mater.* **2017**, *29*, 1702428; b) J. Cheng, L. Liu, G. Liao, Z. Shen, Z. Tan, Y. Xing, X. Li, K. Yang, L. Chen, S. Liu, *J. Mater. Chem. A* **2020**, *8*, 5890-5899; c) B. He, M. Feng, X. Chen, J. Sun, *Green Energy Environ.* **2020**, https://doi.org/10.1016/j.gee.2020.07.011; d) L. Dai, K. Huang, Y. Xia, Z. Xu, *Green Energy Environ.* **2020**, https://doi.org/10.1016/j.gee.2020.09.015.

[13] X. Li, J. Zhang, X. Chen, A. Fischer, A. Thomas, M. Antonietti, X. Wang, *Chem. Mater.* **2011**, *23*, 4344-4348.

[14] Catherine M. Aitchison, R. S. Sprick, A. I. Cooper, *J. Mater. Chem.* A **2019**, *7*, 2490-2496.

[15] a) L. Wang, R. Fernandez-Teran, L. Zhang, D. L. Fernandes, L. Tian, H. Chen, H. Tian, *Angew. Chem. Int. Ed.* **2016**, *55*, 12306-12310; b) P. B. Pati, G. Damas, L. Tian, D. L. A. Fernandes, L. Zhang, I. B. Pehlivan, T. Edvinsson, C. M. Araujo, H. N. Tian, *Energy Environ. Sci.* **2017**, *10*, 1372-1376; c) P. J. Tseng, C. L. Chang, Y. H. Chan, L. Y. Ting, P. Y. Chen, C. H. Liao, M. L. Tsai, H. H. Chou, *ACS Catal.* **2018**, *8*, 7766-7772; d) A. Liu, C.-W. Tai, K. Holá, H. Tian, *J. Mater. Chem. A* **2019**, *7*, 4797-4803. e) M. H. Elsayed, J. Jayakumar, M. Abdellah, T. H. Mansoure, K. Zheng, A. M. Elewa, C. L. Chang, L. Y. Ting, W. C. Lin, H. H. Yu, W. H. Wang, C. C. Chung, H. H. Chou, *Appl. Catal. B-Environ.* **2021**, *283*, 119659; f) A. Liu, L. Gedda, M. Axelsson, M. Pavliuk, K. Edwards, L. Hammarstrom, H. Tian, *J. Am. Chem. Soc.* **2021**, *143*, 2875-2885.

[16] a) C. Dai, M. Panahandeh-Fard, X. Gong, C. Xue, B. Liu, *Solar RRL* **2019**, *3*, 1800255; b) Z. Hu, X. Zhang, Q. Yin, X. Liu, X.-f. Jiang, Z. Chen, X. Yang, F. Huang, Y. Cao, *Nano Energy* **2019**, *60*, 775-783.

[17] D. J. Woods, R. S. Sprick, C. L. Smith, A. J. Cowan, A. I. Cooper, *Adv. Energy Mater.* **2017**, *7*, 1700479.

[18] M. Schwarze, D. Stellmach, M. Schroder, K. Kailasam, R. Reske, A. Thomas, R. Schomacker, *Phys. Chem. Chem. Phys.* **2013**, *15*, 3466-3472.

[19] a) M. Wang, N. Yang, Z. Guo, K. Gu, A. Shao, W. Zhu, Y. Xu, J. Wang, R. K. Prud'homme, X. Guo, *Ind. Eng. Chem. Res.* **2015**, *54*, 4683-4688; b) Y. Liu, C. Cheng, Y. Liu, R. K. Prud'homme, R. O. Fox, *Chem. Eng. Sci.* **2008**, *63*, 2829-2842.

[20] H. Shen, S. Hong, R. K. Prud'homme, Y. Liu, *J. Nanopart. Res.* **2011**, *13*, 4109-4120.

[21] M. Wang, Y. Xu, Y. Liu, K. Gu, J. Tan, P. Shi, D. Yang, Z. Guo, W. Zhu, X. Guo, M. A. Cohen Stuart, *ACS Appl. Mater. Interfaces* **2018**, *10*, 25186-25193.

[22] J. Kosco, M. Bidwell, H. Cha, T. Martin, C. T. Howells, M. Sachs, D. H. Anjum, S. Gonzalez Lopez, L. Zou, A. Wadsworth, W. Zhang, L. Zhang, J. Tellam, R. Sougrat, F. Laquai, D. M. DeLongchamp, J. R. Durrant, I. McCulloch, *Nat. Mater.* **2020**, *19*, 559–565.

[23] T. Hisatomi, J. Kubota, K. Domen, Chem. Soc. Rev. **2014**, 43, 7520-7535.

[24] Z. Hu, Z. Wang, X. Zhang, H. Tang, X. Liu, F. Huang, Y. Cao, *iScience* **2019**, *13*, 33-42.

[25] M. Sachs, H. Cha, J. Kosco, C. M. Aitchison, L. Francas, S. Corby, C. L. Chiang, A. A. Wilson, R. Godin, A. Fahey-Williams, A. I. Cooper, R. S. Sprick, I. McCulloch, J. R. Durrant, *J. Am. Chem. Soc.* **2020**, *142*, 14574-14587.

[26] Z. Fu, A. Vogel, M. A. Zwijnenburg, A. I. Cooper, R. S. Sprick, *J. Mater. Chem. A* **2021**, *9*, 4291-4296.

7

RESEARCH ARTICLE

Entry for the Table of Contents
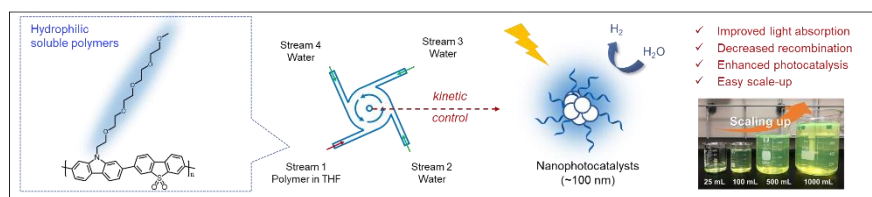
This work presents a novel flash nanoprecipitation (FNP) method with rationally designed hydrophilic polymers to prepare nanoparticulate photocatalysts, which is effective in addressing limitations of bulky particles and greatly improving the photocatalytic activity. More importantly, this nanostructure engineering is promising for scale-up owing to the continuous operation of FNP, which presents a vision for the future practical applications of solar-to-chemical energy conversions.